Characterization of PP/TPV/MMT Ternary Nanocomposites Produced by Injection Molding

Maria A. Costantino,*[1] *Frederico Rueda*,[1] *Valeria Pettarin*,[1] *Patricia M. Frontini*,[1] *Antonio J. Pontes*,[2] *Julio C. Viana*[2]

Summary: One of the most valued and required features of new polymers are a high level of stiffness combined with good toughness. In this way, it seems useful to combine nanoclay reinforcement with rubber toughening to balance end use performance. In this work, the feasibility of producing this kind of nanocomposites by direct injection molding is evaluated. The performance of actual injected pieces of polypropylene (PP) compounded with thermoplastic vulcanizate (TPV) and organoclay (MMT) is analyzed and compared. Ternary composite presents low warpage and so better final quality. Morphology developed in actual pieces is influenced both by processing and by MMT presence, this morphology giving place to alternative deformation mechanisms and crack arrest. Also, a good impact resistance compared with neat PP is observed. Weld lines are diluted and they do not act as stress concentrators, this being of mechanical and aesthetical interest. The use of PP/TPV/MMT seems to be promising for injected moldings.

Keywords: injection molding; mechanical performance; nanoclay; polypropylene thermoplastic vulcanizate

Introduction

While developing new polymers, a high level of stiff and simultaneously tough material behavior is an important goal. Interest in polymer-layered organoclay nanocomposites has been increasing both in industry and in academia, due to their potential for enhanced physical, chemical, and mechanical properties compared to conventionally filled composites. However, reinforcement with organoclays lead generally to reduced ductility and impact resistance. On the other hand, to improve polypropylene (PP) impact performance, elastomeric particles are commonly incorporated into PP, but rubber modification of PP is known to cause dramatic reductions in both strength and stiffness.

Then, it seems useful to combine nanoclay reinforcement with rubber toughening to balance end use performance in terms of toughness and rigidity. Some efforts has been carried out in preceding years towards producing ternary rubber/clay/polymer composites with balanced mechanical properties.[1–3]

The most popular elastomers used to modify PP are ethylene–propylene copolymer (EPR), ethylene–propylene diene terpolymer (EPDM) and ethylene–octene copolymer (EOR).[4–6] An interesting alternative are Thermoplastic Elastomeric Materials (TPE), which have a two-phase structure: an elastomeric phase giving the material rubber-like properties and a stiffer thermoplastic phase (matrix) that melts at elevated temperature making TPE processable by conventional thermoplastic

[1] Institute of Materials Science & Technology (INTEMA) CONICET, University of Mar del Plata, Juan B. Justo 4302, B7608FDQ Mar del Plata, Argentina
E-mail: alejandra-costantino@hotmail.com
[2] Institute for Polymers and Composites, IPC/I3N, Department of Polymer Engineering, University of Minho, Campus de Azurém, 4800-058 Guimaraes, Portugal

techniques. Particularly, thermoplastic vulcanizates (TPV) are a type of TPE prepared by dynamic vulcanization, consisting of the crosslinking of an elastomer during its melt blending with a thermoplastic polymer, and leading to fully vulcanized and finely dispersed rubber droplets in the thermoplastic matrix.[7,8] Furthermore, the TPV has been proposed as improving toughness agent of PP in recent publications.[9,10]

Many PP parts are processed by injection molding that involves a complex flow inside the mold cavity that induces patterns in morphology and microstructure – including high molecular and reinforcement orientation – which can affect part performance. In this type of processing, the occurrence of weld lines is a major design concern as weld lines could lead to a considerable reduction in mechanical properties. While weld lines can be deleterious in homopolymer moldings, the problem can be amplified in multi-phase systems, such as reinforced thermoplastics,[11] and especially for the PP/rubber blends.[12]

In our previous investigations conducted on PP/organoclay nanocomposite moldings – carried out on pieces that included a weld line – we found that nanoclay induces changes in the morphology developed upon processing.[13–15] It enhances molecular orientation induced by flow increasing the level of crystalline phase orientation in the flow direction. To find out the influences of the weld lines and of the complex flow upon final properties, fracture toughness was evaluated at different locations of the parts and a spatial distribution of toughness was found. In samples extracted at bulk positions, a slight tendency towards increasing the ductility and the deformation at break with the increase in nanoclay content was found. On the contrary no improvements were seen at the weldline, which remained as a weak zone. This is due to the clay particles being oriented following materials flow pattern during mould filling phase. An optimum in performance was found for moldings with 3% of clay, since at larger clay contents platelets agglomerate and act as stress concentrators. Cracking along the weld line resulted from less macromolecular interpenetration and chain entanglement, and unfavorable nanoparticle orientation. Weld lines are detrimental to the impact performance due to the macromolecular and nanoparticle flow induced orientations. We proposed a failure mechanism that involves nanoclay delamination and multiple matrix crazing to explain the toughening of PP in the directions where the nanoparticle orientation with respect to loading were adequate.

Some work has been done characterizing thermoplastic polymer/rubber/MMT specimens,[16–22] but no studies regarding actual PP/TPV/nanoclay injected moldings, with real life product features as reduced thickness, long flow paths, radial divergent flows, and formation of weld lines has been reported so far. The influence of processing is critical in the performance of injected products, so a complete characterization and understanding is worthy.

In this work, box-like parts of PP modified with TPV and nanoclay were injection molded. Due to the gating options (hot runner with two gate points), the major box surface shows a central weld line, originated by the top-to-top meeting of the two flow fronts. Warpage and morphology induced by processing was characterized. Mechanical performance was characterized at different locations in the moldings to verify the influence of inhomogeneities and flow pattern upon mechanical behavior.

Experimental Section

Materials, Blends Compounding and Processing

PP homopolymer from DUCOR 3048 TC has a specific gravity of 0.9 g/cm^3 and a melt flow index of MFI = 48 g/10 min (190 °C, 2.16 kg) . High MI was chosen to avoid the expected excessive viscosity of the blend, i.e., to use a temperature profile during injection molding such as not to induce the

thermal degradation of the organo-modifier of the nanoclay. TPV 4775-B40 from Sarlink with specific gravity of 0.91 g/cm^3, apparent shear viscosity of 220 Pa · s (200°C) and hardness of 76 Shore A was used, which is a black, medium hardness, low density thermoplastic vulcanizate suited for injection molding applications that require superior flow properties. Commercial nanoclay from Nanocor, and polypropylene grafted maleic anhydride (PP-g-MA) compatibilizer 427945 from Sigma-Aldrich were also used.

Composites were obtained by direct injection of materials. Pieces of neat PP, PP/TPV (50/50% w/w), PP/TPV/MMT (50/45/5% w/w) and PP/TPV/MMT/PP-g-MA (48.5/45/5/1.5% w/w) were injection molded. In the case of ternary composites, a TPV/MMT masterbatch (90/10% w/w) was prepared previously in a twin-screw extruder and then diluted prior to direct injection moulding.

Two gated boxes of dimensions: 152 mm width, 73 mm length, 16 mm height and 1,6 mm thick were processed in an injection molding machine Ferromatik-Milacron K85 with fixed injection molding parameter (injection temperature = 190 °C; mold temperature = 60 °C; injection speed = 30 mm/s; injection pressure = 58 bar; injection time = 1.29 s; hydraulic packing pressure = 25 bar; packing time = 5 s; cooling time = 30 s).

Dynamic oscillatory shear rheological behavior was evaluated by using an AntonPaar, Physica MCR-301 instrument in parallel- plate geometry with a diameter of 25 mm at 190°C. Measurements were performed with a shear stress amplitude, γ, of 0.1% and frequency range of 0.01–100.

As some difficulties were experienced at the moment of extracting the pieces from the cavity, it was decided to quantify the *friction inside the mold* during part ejection using the experimental technique proposed by Pouzada *et al.*[23] A scheme of the test setup is shown in Figure 1. Friction properties of the molded materials were determined against a surface whose roughness Ra was of 0.7 μm, as measured with a profilometer Phertometer M2. Forces involved in the ejection of an injected part are directly related to the friction coefficient inside the mold, in which replication of the part with the mold roughness is taken into account. Therefore, the determination of the coefficient of friction was done with replication of the mold counter-face (simulating the mold walls) at 40°C (this might being a possible temperature of ejection of the moldings). The contact pressure was set at 600 kPa. The crosshead speed of the Instron machine where the device was mounted was of 100 mm.s^{-1}.

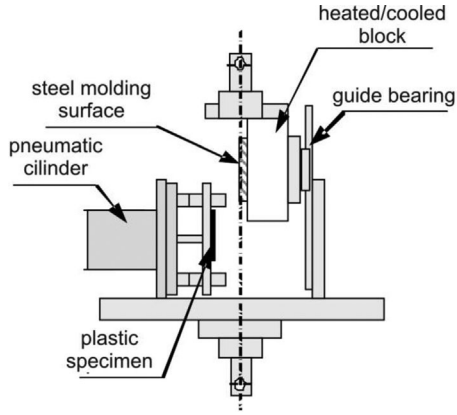

Figure 1.
Scheme of the friction measurement apparatus.

Part Shrinkage Measurements

The shrinkage (S) of moldings was measured on a minimum of three specimens for each condition and in four different zones of the samples: three measurements in the width (w) and one in the length (l). Measurements were done after 24 hours of parts processing with a digital caliper. Parts were stored in controlled temperature and humidity conditions. Shrinkage was determined using the following equations:

$$S_L = \frac{l_M - l}{l_M} \text{ and } S_W = \frac{w_M - w}{w_M} \quad (1)$$

where l and w refers to the length and width of the part; l_M and w_M represents the mold cavity dimensions.

Morphology and Microstructure Characterization

Morphology and microstructure developed of the injected boxes were evaluated by using combined techniques.

Polarized light microscopy (PLM) was used to observe trough the thickness the microstructure of the moldings. 15 μm thick samples were cut with a Leitz 1401 microtome and observed with an Olympus BH2 polarized light microscope.

Differential scanning calorimetry (DSC) tests were performed on specimens that include part of the skin and of the core structure using a Perkin-Elmer equipment at a heating rate of 10° C/min. Melting temperature (T_f) was determined as the endothermic peak temperature.

X-ray diffraction, XRD, analysis was performed on the moldings surface using a Phillips X'PERT MPD diffractometer, in reflection mode (CuKα radiation $\lambda = 1.5418$ Å, generator voltage of 40 kV, current of 40 mA, sample-to-detector distance of 240 mm). Measurements were recorded every 0.02° θ steps for 1 s each, varying 2θ from 2 to 40°. The interlayer distance of the nanoclay was calculated from the (001) peak using the Bragg's law ($\lambda = 2d_{001}\sin\theta_{001}$).The overall crystallinity (Xc) was determined by:

$$X_c = \frac{A_c}{A_c + A_a} \tag{2}$$

where A_c and A_a are the areas under the crystalline peaks andamorphous halo, respectively. The PP α-phase orientation indices were determined according to Trotignon et al.[24]:

$$A_{110} = \frac{I_{110}}{I_{110} + I_{130} + I_{111+041}}; A_{040} = \frac{I_{040}}{I_{110} + I_{040} + I_{130}} \tag{3}$$

where I_α is the peak height after background subtraction.

Samples extracted from various zones of the boxes were cryo-fractured at impact velocities and under liquid nitrogen in order to reveal the microstructures without plastic deformation. Fracture surfaces of broken samples were analyzed using a JEOL JSM-6460LV scanning electron microscope (SEM) at an accelerating voltage of 20 kV. Samples were sputter coated with a thin layer of gold before they were observed. Particle sizes were estimated using Image Pro Plus software.

Transmission electron microscopy (TEM) photographs were obtained with a Jeol 100 CX microscope using an acceleration voltage of 200 kV. Not stained samples were ultramicrotomed at room temperature with a diamond knife to a 70 nm thick section.

Failure Under Tensile Loading

To promote the separation of planes of interest (weld lines, flow lines) mechanical tests were performed under tensile conditions on samples extracted at different locations within the boxes. Two types of samples were used: double edge-sharp notched tensile (DENT) and drilled strips (DS); at two locations: weld line and close to the injection point as depicted in Figure 2. All tests were performed at room temperature. DENT samples were sharp notched and a 2 mm hole was drilled at the centre of the DS samples to induce stress concentration and the breaking of specimens in the same zone where the DENT samples were loaded until fracture at a crosshead speed of 2 mm/min in an Instron 4467 universal testing machine. Sharp notches of a/W = 0.5 were introduced by scalpel-sliding a razor blade having an on-edge tip radius of 13 μm with a Ceast Notchvis notching machine.

DS samples were impacted using a Wollpert standard pendulum fitted with ancillaries for tensile-impact testing at an impact velocity of 3.6 m/s according to ISO 8256. The tensile impact resistance (I_t) was calculated as the total energy to break the specimen divided by the ligament area.

Fracture surfaces of broken samples were analyzed using a JEOL JSM-6460LV scanning electron microscope (SEM) at an accelerating voltage of 20 kV. Samples were sputter coated with a thin layer of gold before they were observed.

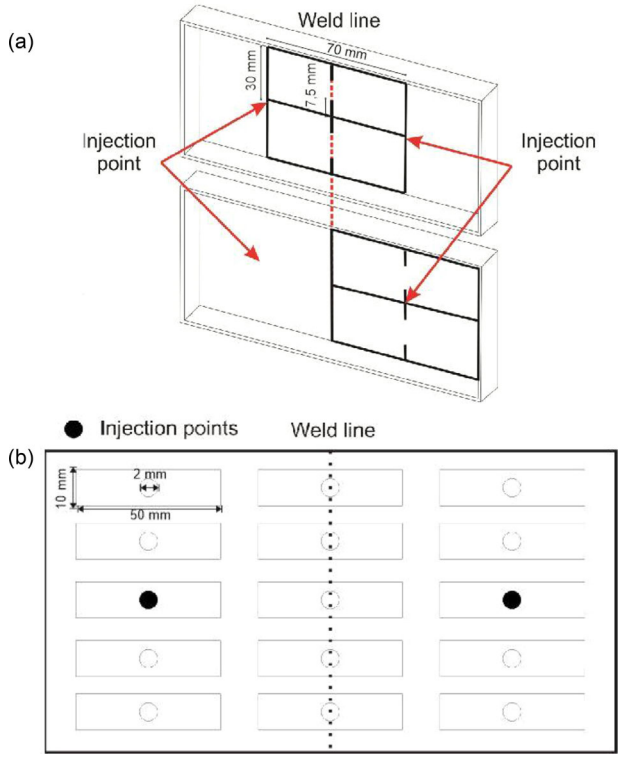

Figure 2.
Scheme of samples used in mechanical characterization (a) DENT. (b) DS.

Results and Discussion

Moldings Characteristics

Typical curves of tests characterizing the friction behavior against mold walls are shown in Figure 3. Presence of TPV increases the friction coefficient from 0.23 (for neat PP) to 0.3, indicating that ejection of pieces from molds involve larger forces, due to the sticky effect of rubber in TPV at high temperatures. Further addition of MMT and compatibilizer did not influence friction inside the mold.

Macroscopic views of the moldings indicated that the presence of TPV also enlarged boxes warpage, while boxes of PP/TPV/MMT exhibited less warpage than neat PP boxes. PP-g-MA counteracted this benefit, enlarging warpage (Figure 4a). Consistently, shrinkage indexes exhibited the same tendency, indicating that PP/TPV/MMT pieces are the ones with higher final quality (Figure 4b). Several authors have also seen this reduction in warpage with nanofillers.[25,26] It has been proposed that nanofillers tend to make the injection-molded parts morphology much more homogeneous, the nucleation being favored instead of crystal growth during the crystallization process, i.e. giving place to smaller spherulites. This reduced material heterogeneity then limits the local differential shrinkage and therefore the parts warpage. Another reason for the warpage reduction noticed upon clay addition may also be that the higher the rigidity of the material is, the less the part is able to deform.

Morphology and Microstructure

Injected parts present the typical skin-shear layer-core structure of injected moldings as seen by PLM (Figure 5). Typical skin-core structure observed for

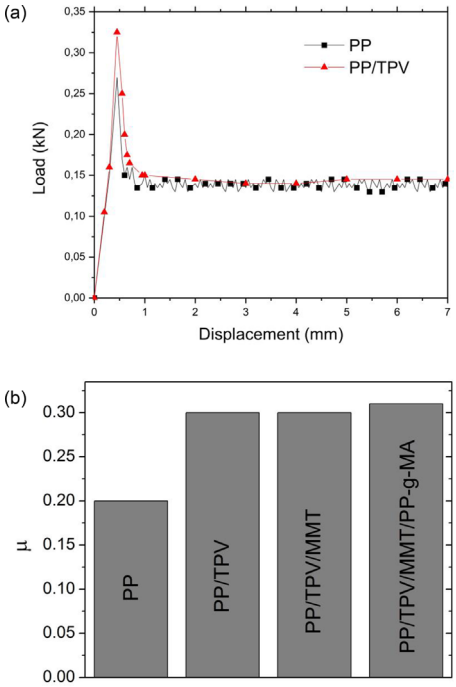

Figure 3.
Results of friction tests with replication of mold roughness (a) Typical curves (b) Friction coefficients obtained.

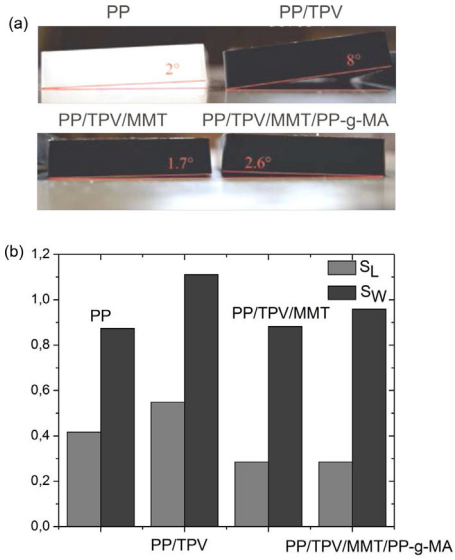

Figure 4.
Boxes characteristics (a) Lateral view of injected boxes along with angle of warpage (b) Shrinkage indexes of boxes.

PP is less noticeable in composites, but it is still present. The incorporation of TPV reduces significantly, or even eliminates, the shear layer. The skin thickness seems to be constant regardless the addition of TPV or MMT. Also, in samples with TPV and MMT, spherulites appear to be of smaller size.

The results of the DSC thermograms are shown in (Table 1). T_f decreases for the composites, this meaning that PP crystallites are of smaller thickness. It is well known in literature that these changes are the consequence of the presence of the rubbery phase, which changes markedly, not only the spherulite structure, but also the size of the spherulite, nucleating and restraining the spherulitic growth in the continuous PP phase.[27–30]

Changes in the peaks of the XRD patterns are observed, with lower peak intensities and larger amorphous halo in composites with TPV (Figure 6), in concordance with calculated lower degrees of crystallinity (Table 1). Blending with TPV induces a less orientated PP crystalline structure in the flow direction, as revealed by the orientation indexes presented in Table 1. MMT and PP-g-MA further diminish this orientation with A_{110} indexes 25% smaller than that of PP. Concerning PP polymorphic phases, it is seen a major presence of α-PP, TPV inducing a slight β-PP polymorph increase. XRD patterns of composites with TPV present peaks at $2\theta = 10°$ and $2\theta > 30°$ Corresponding to additives present in TPV formulation. Intercalated clay agglomerates are evident in the peaks observed at $2\theta = 4.4°$ and $2\theta = 6.4°$, corresponding to platelet interspaces of 2 and 1.38 nm respectively both for PP/TPV/MMT and PP/TPV/MMT/PP-g-MA.

SEM pictures of cryo-fractured samples show the expected two phase microstructure of composites (Figure 7). The dark holes represent the rubbery phase that was torn away during fracture. It is seen that spherical TPV particles are well distributed within composites' core. Particles mean

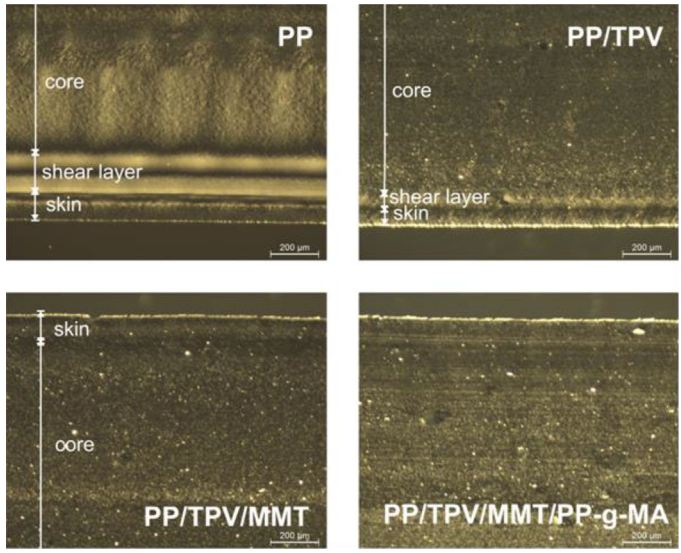

Figure 5.
Typical skin-core structures as seen by polarized optical microscopy.

diameter diminishes from $1.4 \pm 0.5\,\mu m$ in PP/TPV blends to $0.9 \pm 0.5\,\mu m$ in PP/TPV/MMT, a reduction of 35%. PP-g-MA reverts this effect of MMT: TPV particles showing a mean diameter of $1.3 \pm 0.6\,\mu m$. It has been proposed in literature that this decrease in particles diameter may result from two compounding effects present during melt-processing: a) high melt viscosity due to the clay content, controlling the particle size through shear-mixing breakup and coalescence[31]; and b) clay particles that may hinder elastomeric particles coalescence.[32,33] Since viscosity of PP/TPV/MMT and PP/TPV/MMT/PP-g-MA are similar (Figure 8) even though their mean particle diameters are different, it seems that the hindering effect could be the responsible of verified particle size decrease. Also, it can be observed in Figure 8 that the incorporation of MMT almost eliminate the Newtonian plateau for the low angular frequencies, the MMT based composites showing a continuous decrease of the complex viscosity with the angular frequency. At high frequencies the differences between the viscosities of the materials are much less.

Table 1.
Crystalline parameters of PP matrix away from the weld line.

Material	T_f [°C][a]	A_{110}[b]	A_{040}[b]	X_c [%][b]
PP	166	0.48	0.50	48
PP/TPV	162	0.39	0.44	40
PP/TPV/MMT	161	0.37	0.41	36
PP/TPV/MMT/PP-g-MA	160	0.36	0.39	35.5

[a] From DSC.
[b] From DRX.

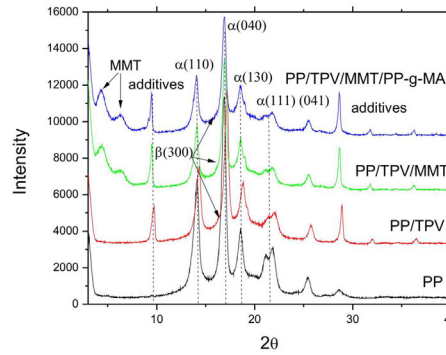

Figure 6.
XRD patterns of all processed materials.

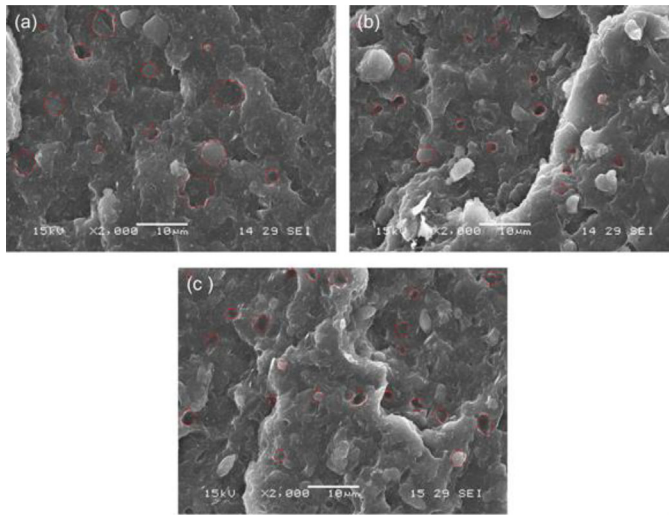

Figure 7.
SEM micrographs of cryo-fractured samples. Some torne away rubber particles are marked with white dot lines as examples (a) PP/TPV; (b) PP/TPV/MMT; (c) PP/TPV/MMT/PP-g-MA.

TEM micrographs show dispersed rubber particles in the PP matrix (Figure 9) throughout the injected boxes. There are practically no morphological differences between the area near the injection point and in the welding zone. On the contrary, there is a slight difference between skin and core parts morphology: skin rubber particles appear to be more elongated and oriented in flow direction while the in the core they appear spherical shaped. This effect is a consequence of the shear profile generated during processing, which presents a maximum in shear near the mold walls and a minimum in the thickness center.

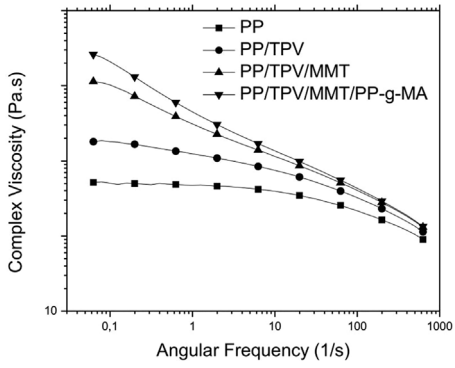

Figure 8.
Viscosity as a function of angular frequency, at 190°C, for all processed materials.

The modification of blends with MMT induces differences in the size of the dispersed rubber particles (as previously seen by SEM). The nanoclay appears in the PP matrix mainly exfoliated with presence of some agglomerates, principally in the area of the injection point There is a strong orientation of nanoparticles in the flow direction in the skin of PP/TPV/MMT, while clay particles are random distributed in the core. PP-g-MA appears to reverse the hindering effect of the nanoclay, generating a similar morphology to that of PP/TPV blends. PP-g-MA does not improve the degree of clay exfoliation (XRD peaks $2\theta = 4.2°$ and $2\theta = 6.2°$, corresponding to platelet interspaces of 2.1 and 1.4 nm, respectively). It is noticed that both PP/TPV/MMT and PP/TPV/MMT/PP-g-MA present similar morphology of rubber particles to that observed for PP/TPV blends, i.e. elongated at skin and rounded in the core. All these features previously described of ternary materials morphology are summarized in Figure 10.

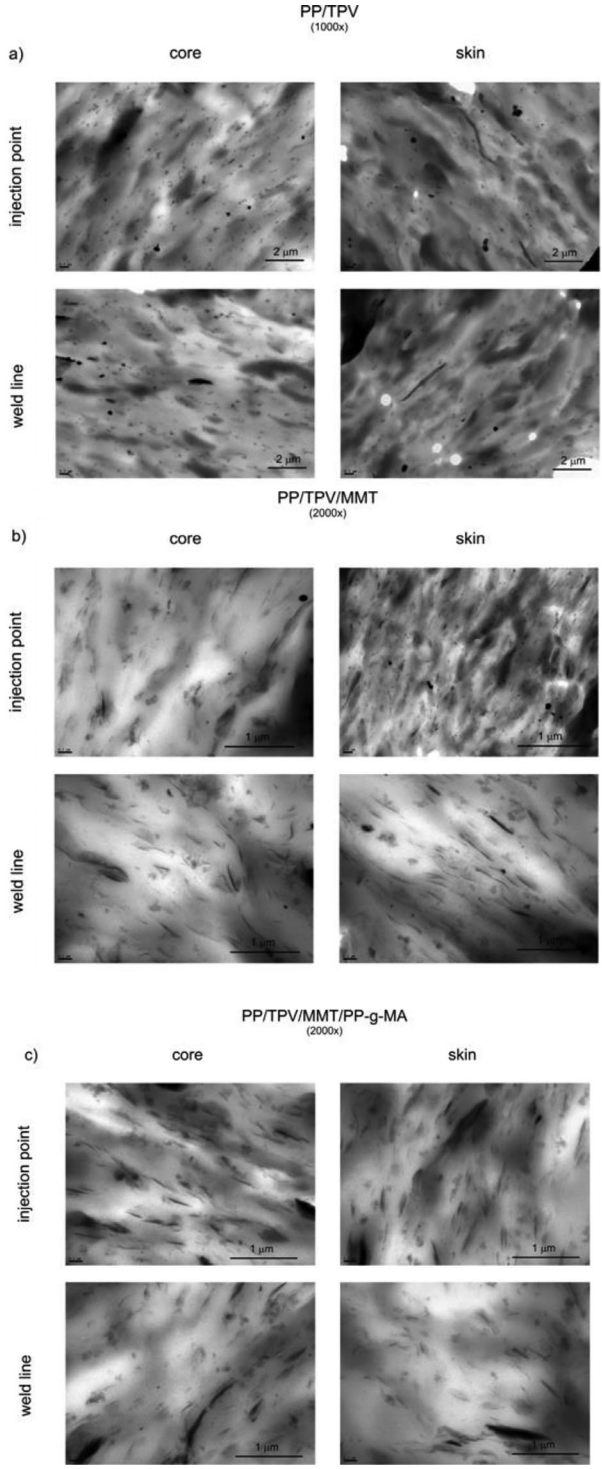

Figure 9.
TEM micrographs at different locations (a) PP/TPV; (b) PP/TPV/MMT; (c) PP/TPV/MMT/PP-g-MA.

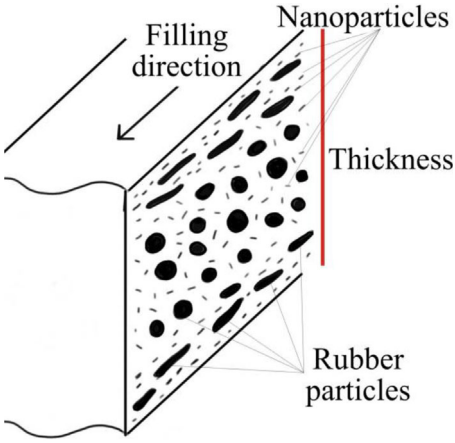

Figure 10.
Scheme of morphology developed during processing in the ternary materials (PP/TPV/MMT).

Failure Under Tensile Loading

Typical load-displacement curves are shown in Figure 11. PP specimens show unstable brittle fracture after reaching the maximum load at small displacement levels, characterized by a slight non-linear load-displacement behavior. Crack failure is accompanied by the occurrence of secondary cracks that follows the flow pattern developed during processing (see inserted photos in Figure 11).

As expected, rubbery phase in TPV promotes a stable behavior with crack tip blunting and specimen whitening in PP/TPV blends. Furthermore, a crack path deviation is seen: the crack does not develop in the plane that contains the initial sharp notch, i.e. the crack path is not controlled by the initial notch, but by the flow pattern (see inserted photos in Figure 11).

PP/TPV/MMT exhibits an apparent stable behavior accompanied by crack tip blunting with no propagation and subsequent arrest of crack and stretching of the inner ligament accompanied by skin delamination. This behavior was reported in literature as a consequence of the specific skin-core structure[34] and it is the responsible of the unrealistic fractures energies involved. Due to this rear failure mechanism it is not possible to determine a fracture toughness following Fracture Mechanics approaches.

PP-g-MA revokes MMT effect and PP/TPV/MMT/PP-g-MA moldings behaves in a way similar to PP/TPV blends.

Fortunately, weld line presence is diluted in composites' performance, indicating that weld line does not act as a weak area, and in concordance with its previous described non-visibility of the weld line.

SEM observations may aid to understand materials behavior. In PP/TPV fracture surfaces stretch marks are observed in the thickness direction (Figure 12). This pattern is originated by a gradual energy release during propagation of small cracks.[35]

Two different and isolated failure mechanisms are observed in the skin and the core of PP/TPV/MMT. The core – with spherical rubber particles and random oriented MMT – shows evidences of cavitation with subsequent shear yielding; while the skin – with elongated rubber particles and MMT particles oriented in the flow direction – is slightly roughened with no signs of cavitation (Figure 13). It is known that elastomeric phase morphology plays a key role in toughness increase.[36–39] Rounded particles favor stress concentration that induces different energy absorption mechanisms (e.g., craze, shear yielding) while elongated particles are not capable of generating the stress field needed to provoke toughening mechanisms.[39] This seems to be the cause of the different behaviors exhibited by the skin and core.

Besides, massive plastic deformation, with high fibrillation is observed in the core region. Saminathan et al. observed that fibrils, when are embedded in intercalated or exfoliated clay layers, have the ability to arrest crack propagation.[40] Furthermore, elongated rubber particles may act as a stopper that contributes to crack arrest by means of crack bridging.

A distinctive feature is that massive craze evidences are seen in the region between the skin and the core (Figure 14).

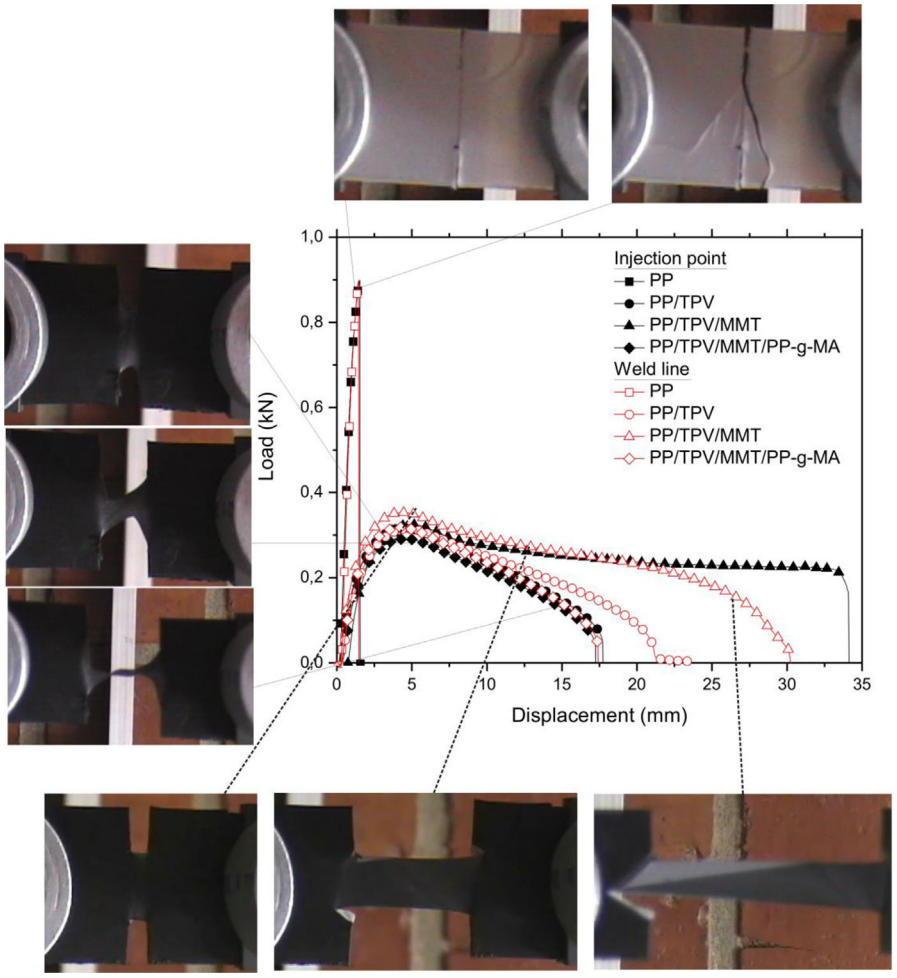

Figure 11.
Typical load–displacement curves and fracture development of composites under quasi-static loading conditions.

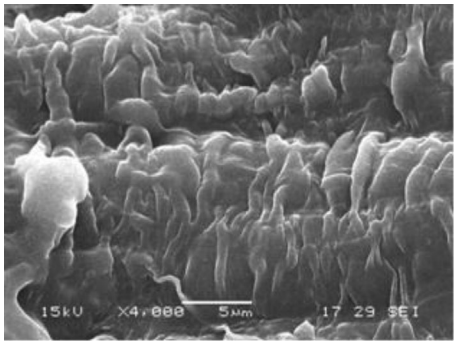

Figure 12.
PP/TPV fracture surfaces under quasi-static loading conditions as seen by SEM.

In PP injected parts, craze mechanisms are generally not seen in the samples' skin,[41] but they can be seen in the shear region located between the skin and core layers.[12] A plausible explanation is that the molecular orientation of skin increases the material resistance to undergo crazing,[41] while columnar morphology, typical of the shear region, enhances the PP matrix ability to experiment crazing. It was pointed out in literature that nanoclay is capable of promoting the development of this columnar structure[16,42,43] and therefore enhances the ability to develop craze. Moreover, the PP ability to develop craze is

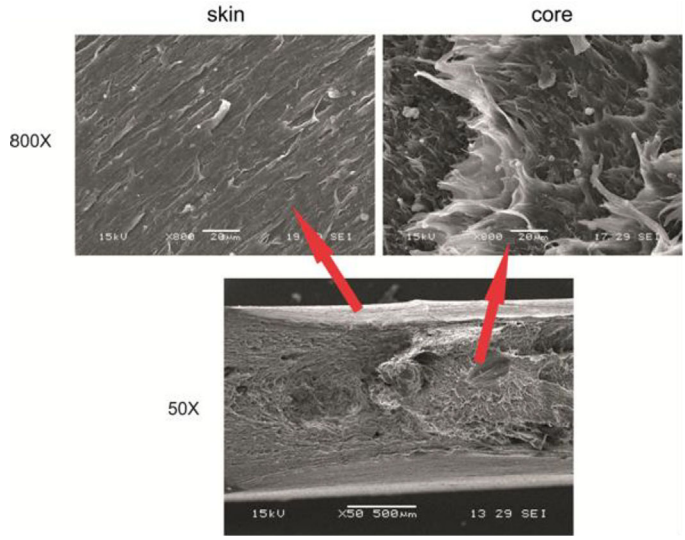

Figure 13.
SEM observations of different failure mechanisms presented in PP/TPV/MMT ternary composites under quasi-static loading conditions.

greatly influenced by rubber particles size: a critical minimum diameter of 0.5 μm is necessary to nucleate crazes in PP; above this critical size, for the same rubber weight fraction a low diameter implies a greater number of potential initiation sites for craze nucleation.[27] Rubber particles present in all composites are larger than critical size, but particles in PP/TPV/MMT are the smallest, i.e., composites with MMT have more initiation sites for craze development. The coalescence of crazes damage in the columnar zone seems to be the responsible of observed skin delamination (as depicted in Figure 15).

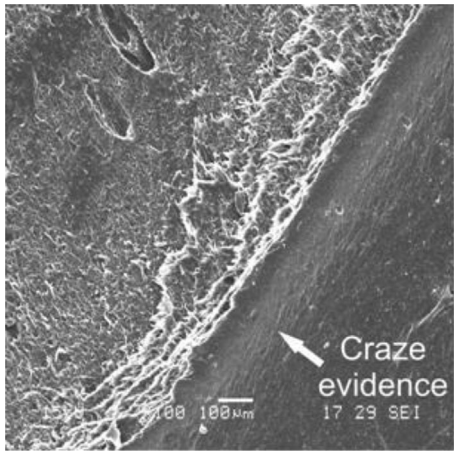

Figure 14.
Craze evidences in PP/TPV/MMT under quasi-static loading conditions as seen by SEM.

Mechanisms generated by nanoclay are suppressed by the presence of PP-g-MA. This is probably due to the clay agglomeration (Figure 16) related to the migration of compatibilizer to the surface of the pieces that pushes the nanoclay also to the surface of the specimens, as previously seen for PP/MMT injected composites.[14]

Tensile impact resistances (I_t) are summarized in Table 2. Results are similar for injection point and weld line zones, reinforcing the idea that weld line does not act as a defect, in this particular case. TPV increases I_t of PP in 500%. MMT diminishes I_t of PP/TPV/MMT as compared with PP/TPV. However, if compared with PP, PP/TPV/MMT displays a 300% larger I_t. The presence of PP-g-MA partially inhibits the effect of MMT.

SEM micrographs show three different behaviors (Figure 17). PP exhibits a

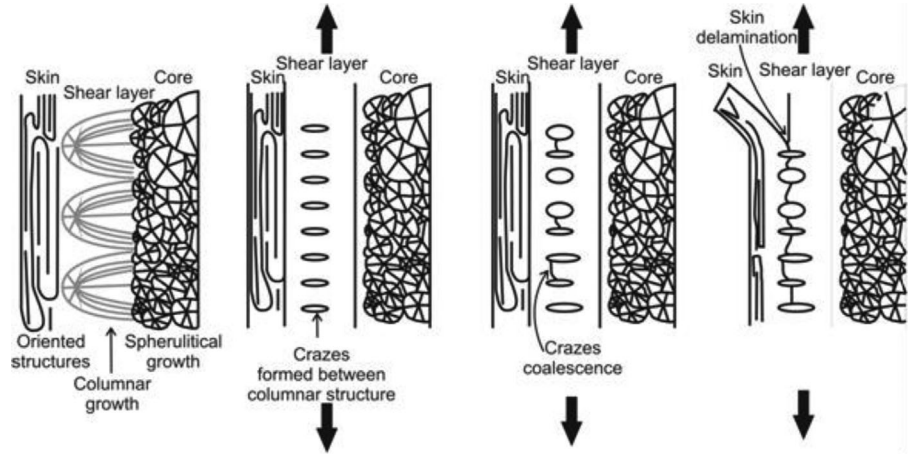

Figure 15.
Scheme of PP microstructure in injected PP/TPV/MMT composites and development of crazes in the columnar zone under quasi-static loading conditions.

completely brittle fracture surface characterized by cleavage planes. A competition is observed between two dissimilar failure mechanisms in composite materials: one with different mechanisms in the skin and core (both zones with plastic deformation that involves large energy consumption); and another in which differentiation is inhibited and a brittle failure mechanism with removed rubber particles in all fracture surfaces (skin and core) occurs. PP/TPV samples show mostly the first type of failure, while PP/TPV/MMT and PP/TPV/MMT/PP-g-MA exhibit mostly the second type, this being the cause of differences observed in absorbed energy.

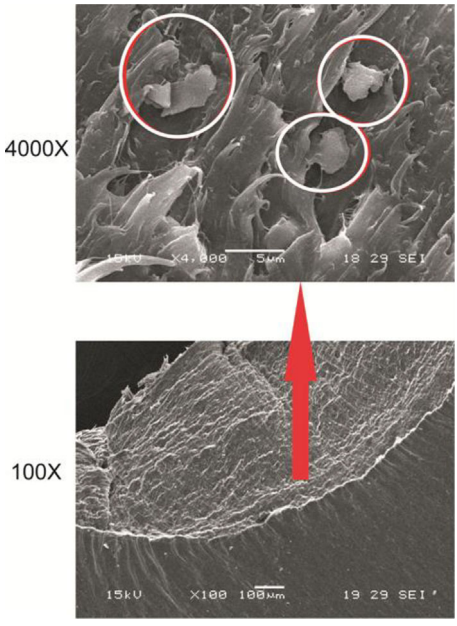

Figure 16.
Failure mechanisms observed in PP/TPV/MMT/PP-g-MA injected composites under quasi-static loading conditions.

Conclusions

In this work, the feasibility of producing nanocomposites by injection molding is evaluated. The performance of PP, PP/TPV, PP/TPV/MMT and PP/TPV/MMT/PP-g-MA composites manufactured by injection molding is analyzed and compared. Main findings are summarized as follows.

TPV increases friction coefficient inside the mold at high temperature, so increasing ejection load during molding process. It also enlarges warpage in boxes like moldings produced. However, MMT diminishes PP/TPV/MMT boxes deformation below

Table 2.
Tensile impact resistance.

Impact energy [kJ/m^2]	PP	PP/TPV	PP/TPV/MMT	PP/TPV/MMT/PP-g-MA
Injection point	29 (±10)	148 (±17)	77 (±2)	111 (±11)
Weld line	28 (±10)	146 (±10)	81 (±13)	90 (±17)

the one of PP. PP/TPV/MMT pieces are the ones with higher final quality.

Two types of rubber morphology are seen: elongated in the skin and round shaped in the core regions, due to the through-the-thickness shear profile during injection processing. Besides, MMT generates differences, hindering elastomeric particles coalescence and so reducing its shape in 35%.

In respect to the mechanical properties, fracture regime is dependent on the type of material and its morphology (rubber shape + orientation, and MMT orientation) generated during processing: PP exhibits brittle fracture behavior; PP/TPV and PP/TPV/MMT/PP-g-MA show plastic behavior with controlled crack propagation; and PP/TPV/MMT is characterized by crack blunting and arrest. Under impact conditions, TPV highly enlarges energy consumed during fracture, as expected. MMT detriments impact resistance of PP/TPV/MMT as compared to PP/TPV, but it is still 300% larger that energy consumed by

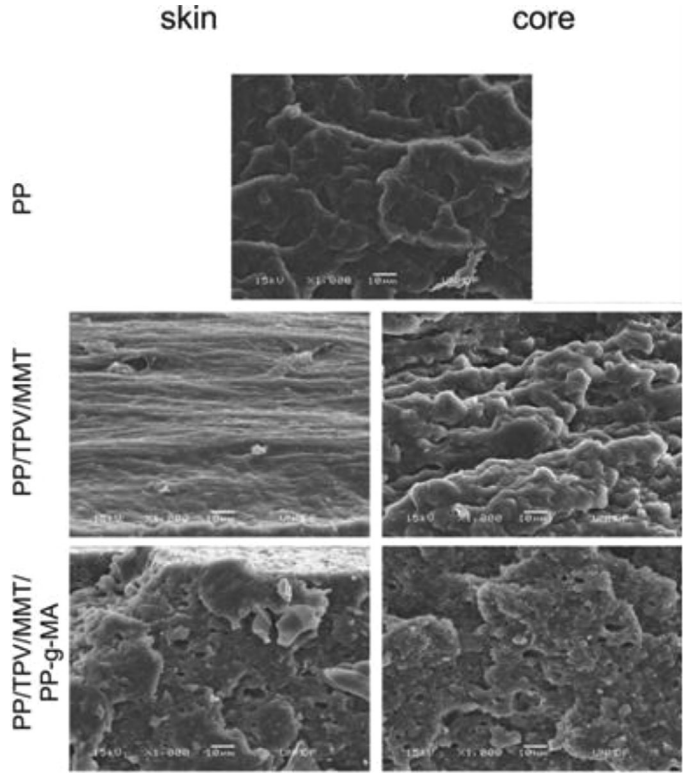

Figure 17.
SEM observations of failure mechanisms under impact conditions of injected composites.

neat PP. Fortunately, weld lines are diluted and they do not act as stress concentrators, this being of mechanical and aesthetical interest.

In conclusion, the use of PP/TPV/MMT is promising for injected moldings. Positive aspects are: low warpage, crack arrest, good impact resistance compared with neat PP and no need of compatibilizer. However, it should be taken into account that the injection cycle is slightly increased due to difficulties in parts ejection and skin delamination occurs at higher deformations.

Acknowledgements: Authors would like to thank CONICET, ANPCyT and UNMdP from Argentina and University of Minho from Portugal for financial support. Alejandra Costantino developed part of this work under a Bec. Ar grant (Argentinean Government).

[1] J. Jancar, A. T. Dibenedetto, *J. Mater. Sci.* **1994**, *29*, 4651.
[2] J. Jancar, A. T. Dibenedetto, *J. Mater. Sci.* **1995**, *30*, 2438.
[3] C. G. Ma, Y. L. Mai, M. Z. Rong, W. H. Ruan, M. Q. Zhang, *Comp. Sci. Technol.* **2007**, *67*, 2997.
[4] B. K. Kim, M. S. Kim, K. J. Kim, *J. Appl. Polym. Sci.* **1993**, *48*, 1271.
[5] S. C. Tjong, Y. Z. Meng, *J. Polym. Sci. Part B: Polym. Phys.* **2003**, *41*, 2332.
[6] S. Molnár, B. Pukánsky, C. Hammer, F. H. J. Maurer, *Polymer* **2000**, *41*, 1529.
[7] M. D. Ellul, A. H. Tsou, W. Hu, *Polymer* **2004**, *45*, 3351.
[8] C. Harrats, S. Thomas, G. Groeninckx, Micro- and Nanostructured Multiphase Polymer Blend Systems: Phase Morphology and Interfaces, 2005. https://www.crcpress.com/Micro-and-Nanostructured-Multiphase-Polymer-Blend-Systems-Phase-Morphology/Harrats-Thomas-Groeninckx/p/book/9780849337345.
[9] R. Keskin, S. Adanur, *Polym.-Plastics Technol. Eng.* **2011**, *50*, 20.
[10] L.-F. Ma, W.-K. Wang, R.-Y. Bao, W. Yang, B.-H. Xie, M.-B. Yang, *Mater. Design.* **2013**, *51*, 536.
[11] D. M. Bigg, "6 — Properties and processing of short metal fibre filled polymer composites", in *Short Fibre–Polymer Composites*, Woodhead Publishing, Cambridge, **1996**, pp. 144–167.
[12] J. Karger-Kocsis, I. Csikai, *Polym. Eng. Sci.* **1987**, *27*, 241.
[13] V. Pettarin, G. Viau, L. Fasce, J. C. Viana, A. J. Pontes, P. M. Frontini, A. S. Pouzada, *Polym. Eng. Sci.* **2013**, *53*, 724.
[14] A. Costantino, V. Pettarin, J. Viana, A. Pontes, A. Pouzada, P. Frontini, *Polym. Int.* **2013**, *62*, 1589.
[15] V. Pettarin, F. Brun, J. C. Viana, A. S. Pouzada, P. M. Frontini, *Comp. Sci. Technol.* **2013**, *74*, 28.
[16] R. Vasudev, V. Abitha, *Pop. Plast. Packag.* **2014**, *59*, 21.
[17] G. Naderi, R. Khosrokhavar, S. Shokoohi, G. R. Bakhshandeh, M. H. R. Ghoreishy, *J. Vinyl Additive Technol.* **2016**, *22*, 320.
[18] A. Dasari, Z.-Z. Yu, Y.-W. Mai, *Polymer* **2005**, *46*, 5986.
[19] W. Dong, X. Zhang, Y. Liu, H. Gui, Q. Wang, J. Gao, Z. Song, J. Lai, F. Huang, J. Qiao, *Eur. Polym. J.* **2006**, *42*, 2515.
[20] A. Dasari, Z.-Z. Yu, M. Yang, Q.-X. Zhang, X.-L. Xie, Y.-W. Mai, *Comp. Sci. Technol.* **2006**, *66*, 3097.
[21] S. Bagheri-Kazemabad, D. Fox, Y. Chen, L. M. Geever, A. Khavandi, R. Bagheri, C. L. Higginbotham, H. Zhang, B. Chen, *Comp. Sci. Technol.* **2012**, *72*, 1697.
[22] C. G. Martins, N. M. Larocca, D. R. Paul, L. A. Pessan, *Polymer* **2009**, *50*, 1743.
[23] A. S. Pouzada, E. C. Ferreira, A. J. Pontes, *Polym. Test.* **2006**, *25*, 1017.
[24] J. P. Trotignon, J. L. Lebrun, J. Verdu, *Plast. Rubber Comp.* **1982**, *2*, 247.
[25] A. M. Cadena-Perez, I. Yañez-Flores, S. Sanchez-Valdes, O. S. Rodriguez-Fernandez, S. Fernandez-Tavizon, L. F. R. de Valle, T. Lozano-Ramirez, J. G. Martinez-Colunga, J. L. Sanchez-Cuevas, *Int. J. Mater. Form.* **2015**, *8*, 1.
[26] S. Fourdrin, J. Soulestin, E. Lafranche, M. Lacrampe, P. Krawczak, Dimensional accuracy and stability of polypropylene-clay nanocomposites injection mouldings, in: PPS-23, The Polymer Processing Society 23rd Annual Meeting, Salvador, Brasil, **2007** pp. P03–040.
[27] B. Z. Jang, D. R. Uhlmann, J. B. V. Sande, *J. Appl. Polym. Sci.* **1984**, *29*, 4377.
[28] B. Z. Jang, D. R. Uhlmann, J. B. V. Sande, *J. Appl. Polym. Sci.* **1985**, *30*, 2485.
[29] J. Z. Liang, R. K. Y. Li, *J. Appl. Polym. Sci.* **2000**, *77*, 409.
[30] X. H. Chen, C. Q. Hu, H. B. Yan, C. Q. Li, X. J. Ling, *Plast. Rubber Comp.* **2009**, *38*, 183.
[31] S. Mehta, F. M. Mirabella, K. Rufener, A. Bafna, *J. Appl. Polym. Sci.* **2004**, *92*, 928.
[32] I. Hejazi, F. Sharif, H. Garmabi, *Mater. Design.* **2011**, *32*, 3803.
[33] B. B. Khatua, D. J. Lee, H. Y. Kim, J. K. Kim, *Macromolecules* **2004**, *37*, 2454.
[34] J. Karger-Kocsis, D. E. Mouzakis, *Polym. Eng. Sci.* **1999**, *39*, 1365.
[35] R. Gensler, C. J. G. Plummer, C. Grein, H.-H. Kausch, *Polymer* **2000**, *41*, 3809.
[36] J. W. Lim, A. Hassan, A. R. Rahmat, M. U. Wahit, *Polym. Int.* **2006**, *55*, 204.
[37] A. Dasari, Q.-X. Zhang, Z.-Z. Yu, Y.-W. Mai, *Macromolecules* **2010**, *43*, 5734.
[38] R. R. Tiwari, D. R. Paul, *Polymer* **2011**, *52*, 4955.

[39] H. Du, Y. Zhang, H. Liu, K. Liu, M. Jin, X. Li, J. Zhang, *Polymer* **2014**, *55*, 5001.
[40] K. Saminathan, P. Selvakumar, N. Bhatnagar, *Polym. Test.* **2008**, *27*, 453.
[41] K. Nitta, Y. Yamamoto, *E-Polymers* **2003**, 3.
[42] Polypropylene Structure, Blends and Composites — Structure and Morphology, Karger Kocsis, Joseph, Ed., Chapman and Hall, London, **1995**.
[43] N. Sheng, M. C. Boyce, D. M. Parks, G. C. Rutledge, J. I. Abes, R. E. Cohen, *Polymer* **2004**, *45*, 487.

